Synchrotron-based X-ray tomographic images and segmentation techniques to account for effects of grain contacts and micro-cracks on rock properties

Kathleen Sell – JGU Mainz, Germany

Claudio Madonna, Beatriz Quintal, Marcel Frehner, Nicola Tisato, and Erik H. Saenger* – ETH Zurich, Switzerland

Abstract

Synchrotron radiation X-ray tomographic microscopy provides ultra-high-resolution 3D digital images of rock microstructures. We describe this method and, to demonstrate its wide applicability, we present 3D images of very different rock types: Berea sandstone, Fontainebleau sandstone, dolomite, calcitic dolomite, and three-phase magmatic glasses. For some samples, full and partial saturation scenarios are considered using oil, water, and air. We provide the raw image data sets as online supplementary material, along with laboratory data describing the rock properties. By making these data sets available to other research groups, we aim to stimulate work based on digital rock images of high quality and high resolution. We also present results from an image segmentation workflow with subsequent computation of permeability and velocities.

Introduction

Three-dimensional (3D) information of microstructures of a rock sample is important for better understanding physical phenomena and for rock characterization at the micro-scale (Madonna et al., 2012). Various methods for obtaining a 3D image of the rock microstructure exist (Madonna et al., 2013, and references therein). They can be separated into two major groups: destructive and non-destructive methods. If possible, the latter is preferable because the same rock sample can be used for further investigations after imaging, for example in laboratory testing. This allows a direct comparison between laboratory tests and calculations based on a digital rock image. The most common non-destructive 3D imaging method for earth sciences is X-ray computed tomography (CT). There is a clear trade-off between sample size and resolution (Figure 1). For each single material sample, it has to be clarified if the chosen sample size is representative for the given task to be considered. In the last decade, the X-ray micro-computed tomography (micro-CT) method became widely available and many modern studies have made use of it to obtain 3D rock images. The resolution of micro-CT is high enough to image the spatial distribution of grains, pores, and pore fluids.
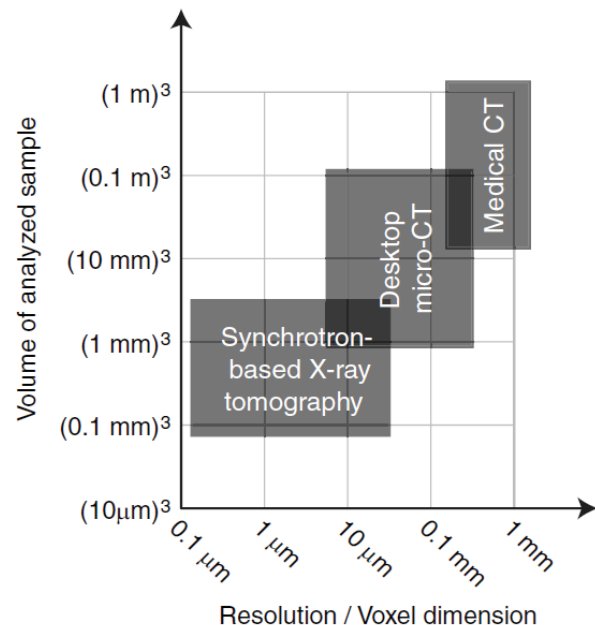
Figure 1. Schematic representation of sample size versus resolution of the most common X-ray computed tomography methods. Other methods are available, but are not plotted here.

Additionally, 3D rock images (Figure 2) can be used for predicting properties such as porosity, permeability, pore size distribution, effective elastic moduli, or electrical conductivity. For example, permeability can be successfully predicted by numerically simulating fluid flow through 3D rock models, with the numerical results being in reasonable agreement with laboratory measurements. In this case, the resolution of the micro-CT technique is sufficient because fluid pathways predominantly follow larger pores. However, if the porosity is much smaller than 1µm (e.g., shale) the agreement might be less satisfactory because of resolution limitations. On the other hand, mechanical properties, such as the effective elastic moduli, strongly depend on the microstructural details of the rock, which stay unresolved by the micro-CT technique. The inability to fully characterize the microstructural details of a rock can lead to disagreements between numerical estimates of mechanical properties based on micro-CT images and laboratory data. Dvorkin et al. (2011) suggested considering trends formed by data points from computational and laboratory measurements, instead of direct point-to-point comparisons.
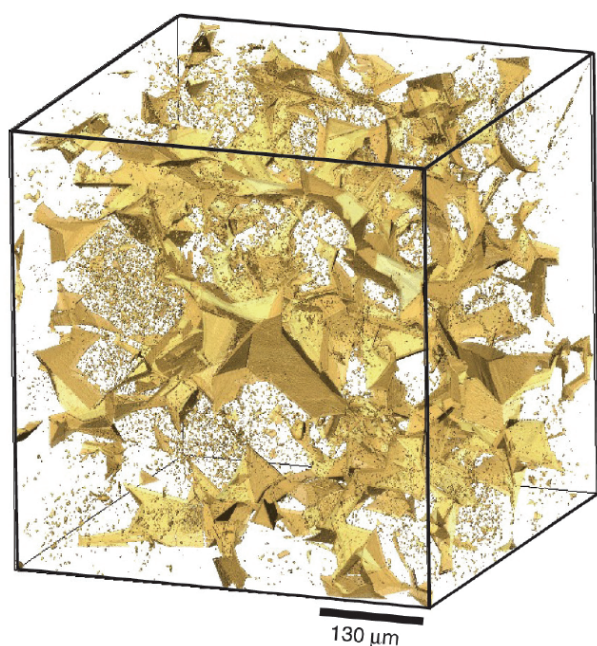
Figure 2. 3D visualization of the pore space of dry Fontaineblue sandstone depicted in yellow using a SRXTM image. The quartz grains are not shown.

The limitations of traditional X-ray micro-CT instruments in fully characterizing the microstructural details of rocks can be significantly reduced by using third-generation synchrotron sources, thanks to their exceptional photon density. The high brilliance of third-generation synchrotron radiation provides increased spatial and temporal resolution. Brilliance (i.e., light intensity) is defined as the number of photons per second per unit source area, emitted per solid angle within a certain wavelength band. The detection of details as small as 1 micron in millimeter-sized samples is routinely possible within only a few minutes. In addition, the monochromaticity of the X-ray beam allows for quantitative measurements of material properties (e.g., density) and simplifies the identification of the different X-rayed phases, because beam hardening artifacts, distinctive for micro-CT setups, can be avoided. Increased contrast and reduced noise are also promoted by the monochromatic beam and the high photon flux. All of these factors result in ultrahigh-resolution images of astonishing quality, which allow a much more detailed analysis compared to micro-CT images.

For this paper, we have employed synchrotron radiation X-ray tomographic microscopy (SRXTM) to obtain high-resolution 3D images of samples of: Dry and water-saturated Fontainebleau sandstone; dry and partially saturated (with two or three fluid phases) Berea sandstone; dry dolomite and calcitic dolomite; three-phase magmatic glass and high-temperature vesiculating magma. We chose such a wide range of different rock samples to demonstrate the power and versatility of the SRXTM-method. On one hand, we deliver images of two standard rocks, Berea and Fontainebleau sandstones, which are often considered as analog rocks for siliciclastic reservoirs and are therefore intensively studied and

characterized. On the other hand, imaging magmatic glass and magma demonstrates the wide applicability of the method also to nonporous materials. The SRXTM-methodology and the resulting images are described and shown in the following sections.

We provide the raw data of all the images (http://www.rockphysics.ethz.ch/downloads) as an incentive to the development of rock physics research using high-resolution digital rock images, which have been of scarce access to a broad scientific community. More details about the described datasets can be found in Madonna et al. (2013).

Despite increased spatial resolution, compared to traditional X-ray micro-CT, the SRXTM-images still demand careful segmentation efforts for subsequent numerical determination of petrophysical properties. Since a representative volume of a porous rock was scanned, the smallest pores, microcracks, and grain-to-grain contacts stay unresolved. For image segmentation and computations of petrophysical properties, we used 3D images of a Berea Sandstone specimen. We analyzed the impact of image processing on subsequent digital rock modeling comprising the determination of porosity, permeability and P-wave velocity.

Case studies

The presented rock images exploit the absorption contrast of the synchrotron beam in gray values. The brighter the gray value is, the higher the absorption of the beam was. To a first order, the absorption is proportional to the material density. Sometimes, the single phases can be easily detected by eye when scrolling through neighboring slices. For a quantitative analysis, each phase of interest has to be identified in the data. This is normally done by attributing a certain range of gray values to a particular phase and is called segmentation. The process of segmentation itself is a subject of current research and is discussed, for example, by Iassonov et al. (2009). Here, we provide and explain the raw data sets. Due to the experimental setup at the TOMCAT synchrotron beam-line, the data in an inner volume of the data cube will provide highest quality. This region is marked as a white dashed circle in the figures showing raw data (Figures 3 and 4). The corners contain artifacts due to less complete data related to the rotation symmetry inherent in tomography. For an accurate analysis, we suggest to preferably use the data within the marked region.

Case 1: Fontainebleau sandstone

A dry sample of Fontainebleau sandstone was imaged with the experimental conditions given in Table 1. Fontainebleau sandstone is often referred to as an analog rock for siliciclastic hydrocarbon reservoirs and has already been investigated in other digital rock studies. The average porosity of our sample is 5.1 vol%. A 3D view of the segmented pore space is shown in Figure 2.

Case 2: Water-saturated Fontainebleau sandstone

The second image of Fontainebleau sandstone is from the same rock sample as the first image. The specific 2 mm diameter specimen was saturated through imbibition.
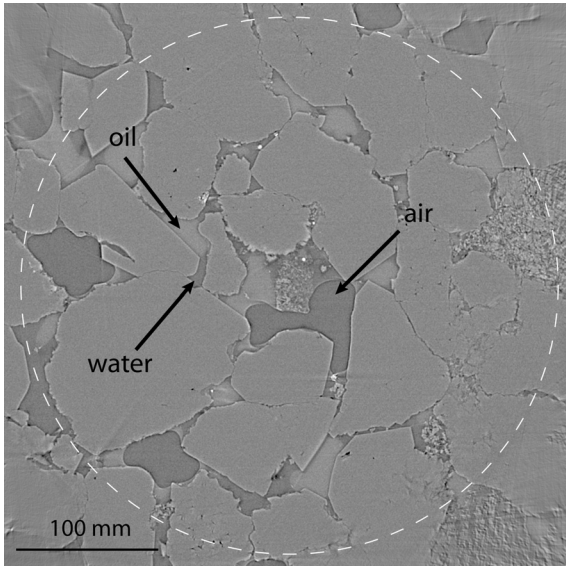
Case 3: Dry Berea sandstone

For the imaging and laboratory experiments of Berea sandstone, a sample from the Berea Sandstone™ Petroleum Cores (Ohio, USA) was used. Berea sandstone is also frequently used as analog rock for siliciclastic hydrocarbon reservoirs and, therefore, is well studied and characterized. The connected porosity of the used sample is around 20%. Permeability as provided by the company is between 200 and 500 mD.

Case 4: Different saturation scenarios of Berea sandstone

In this experiment, another specimen of Berea sandstone from the same block is imaged for three subsequent saturation scenarios. With the same imbibition technique, we saturated the Berea sandstone sample with Angiofil oil. After the first scan of the almost fully oil-saturated Berea sandstone, our aim was to create partially saturated stages with the same specimen. A four-step technique was employed: (1) The specimen was enveloped in a ~2 mm inner diameter polyolefin shrink tube. (2) The specimen was placed inside one end of a 3 mm inner diameter, ~10 cm long latex pipe. (3) The other end of the pipe was connected to a 10 ml syringe filled with the new liquid. (4) Acting on the syringe piston, a flux of liquid was forced to flow through the specimen.

This technique was subsequently applied twice to our specimen. First, we injected air, which pushed the oil out of the pore space. As a result, two phases, air and oil, occupied the connected pores. Second, we injected water. Hence, three phases were expected in the pore space; water, air, and oil (Figure 3).
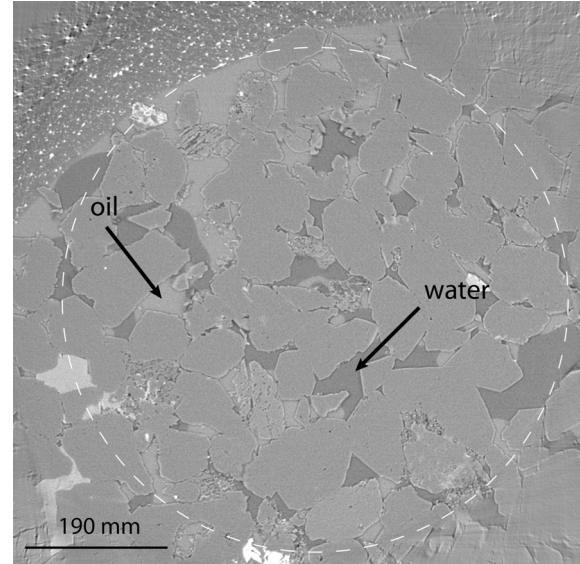

Figure 3. Raw SRXTM-images of Berea sandstone partially saturated with water, air, and oil. The full data cube contains 1024³ voxels with a voxel size of 0.38 µm^3.

Case 5: Another saturation scenario of Berea sandstone

Using a small vacuum pump, a dry sample of Berea sandstone was first saturated with the same Angiofil oil as

in Case 4, and subsequently with water, which leads to a partial saturation of oil and water. This procedure completes the different saturation scenarios described in the previous case. In contrast to Case 4, we have only two saturating phases, oil and water, and a lower magnification, hence a bigger field of view as shown in Figure 4.

Figure 4. Raw SRXTM-images of Berea sandstone partially saturated with water and oil. The full data cube contains 1024³ voxels with a voxel size of 0.74 µm^3.

Cases 6 and 7: Dry carbonate

Image data sets for two dry carbonate rock specimens that originate from a core drilled in northern Switzerland.

Case 8: Three-phase magmatic glass

A synthetic three-phase magmatic glass was deformed in torsion configuration at 200 MPa and 450°C using a Paterson gas-medium apparatus.

Case 9: Magma foaming

To constrain in 3D the effect of water on the process of volatile exsolution (nucleation, growth and coalescence of gas bubble), a natural water-poor, crystal-free phonolitic obsidian from La Cañadas Caldera (Tenerife, Spain) was imaged during a high-temperature experiment.

Image segmentation

Our digital rock physics workflow is illustrated in Figure 5. We focus on the effect of image enhancement techniques and segmentation to complement the paper of Madonna et al. (2012), which compares laboratory measurements of ultrasonic P-wave velocities with digital rock physics results. Image enhancement and segmentation steps were carried out using the software package Avizo Fire 7.0 from VSG (Mérignac, France).

A region of interest (ROI), called Ber1, of 400³ voxels size was chosen from the original data set from Case 3.
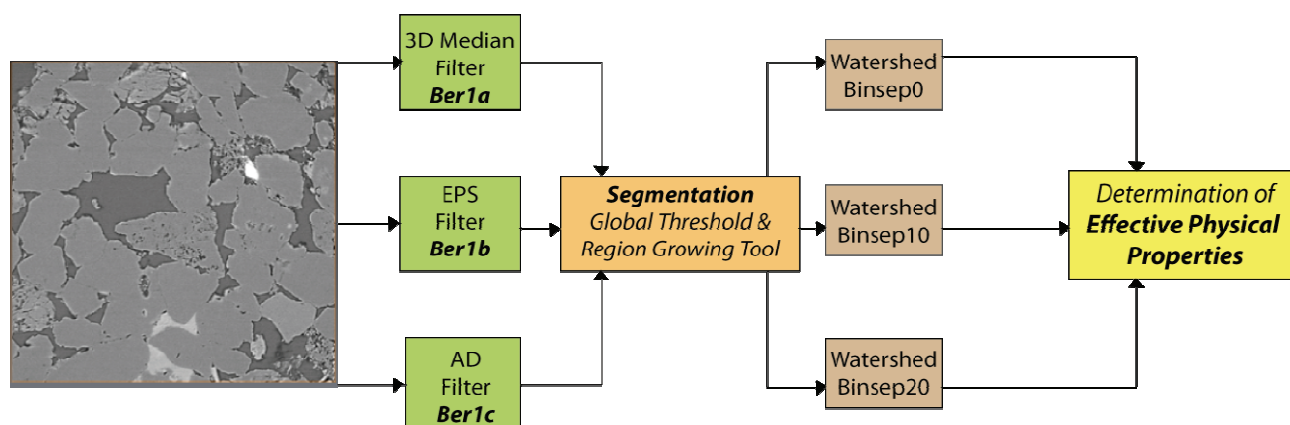
Figure 5. Simplified processing workflow with the raw data Ber1.

The first step in pre-processing was to reduce image noise and scan artifacts using three common image filters, calibrated for the appropriate dimensions and kernel window sizes. Every step of image enhancement changes the original data set affecting subsequent steps required for data analysis. For the first case (Ber1a), a 3D-median filter (3DM) was executed to substitute voxels by calculating a mean value of neighboring voxels subsequently followed by their replacement. For the second scenario (Ber1b), an edge preserve smoothing (EPS) filter was applied. The EPS filter is based on the Sobel operator which preserves grain boundaries by searching for the most homogeneous feature of the input data and assigns the averaged value to an elementary volume (Shulakova et al., 2013). The EPS filter highlights boundaries between different materials. An anisotropic diffusion filter (AD) was exerted for the purpose of image enhancement resulting in the data set Ber1c. In this study the filters were not used in a combined manner to assess the influence of each filter.

The segmentation process includes the transformation of voxels of certain gray value range by using a combination of the global threshold and region growing technique to classify features like phase distributions (e.g. Ianossov et al., 2009). Initially each image enhanced dataset was segmented into three classes: pores, quartz and carbonates (Table 2). These classes were chosen to reproduce the mineral composition known from thin section analysis. To reveal unresolved grain boundaries of the quartz and carbonates the binseparate function was applied to the segmented quartz and carbonate classes. In principle, this command computes watershed lines to separate agglomerated features. Binseparation is a high-level combination of the fast watershed, distance and numerical reconstruction algorithms. In our study, the default values 0, 10 and 20 were selected which revealed crucial differences in trend and quantity of the grain boundaries (Figure 6).

Computing permeability

In principle, fluid flow simulation at the pore-scale can lead to the estimation of permeability when simulating Newtonian fluid flow in the earlier segmented pore space. In this study, the flow simulation based on the Finite Volume Explicit Jump (EJ) method was applied using the GeoDict software package (Math2Market GmbH, Germany), for which the Stokes Equations are solved on an equidistant Cartesian grid on a box-shaped domain for a given pressure drop. The permeability K acts as a material property. Boundary conditions were set to periodic on mirrored domain respectively for each flow direction. The resulting permeability tensor $K(x,y,z)$ is independent of the applied pressure drop and fluid viscosity.

Computing velocities

A series of numerical experiments based on assigned grain-to-grain contacts (Table 2) has been conducted to obtain the effective velocity of the dry rock sample. We applied the rotated staggered finite-difference method appropriate for dynamic measurements. This approach studies the wave propagation in heterogeneous materials within the long wavelength limit. The fundamental idea of the model is discussed in detail by Saenger (2008). On the top of the 3D rock model a body force plane source is applied using a homogeneous buffer zone of assigned vacuum. The plane wave travels through the embedded digitized 3D rock. Two plane receivers on the top and the bottom of the model measure the time-delay of the plane wave's peak amplitude caused by the inhomogeneity of the rock. Effective velocities are determined by comparing the model results with the results of a reference model. The applied input parameters are listed in Table 2. The majority of the grains in Berea sandstone are cemented by fine-crystallized SiO_2 hence a reduced quartz mineral module was assigned for the grain-to-grain contacts (Madonna et al., 2012).

Discussion

For the purpose of image enhancement and noise reduction three filters were applied to a high-resolution 3D rock image with different effects on the output. The 3D Median smoothing filter and the Anisotropic Diffusion filter blurred fine details and tended to smear grain edges, which made it more difficult to distinguish between objects. Especially for regions of the sample where weathered objects like carbonates occurred, it was difficult to segment every small feature even at the spatial resolution of 0.74 μm. The total porosities varied from

12% for the unfiltered dataset Ber1 to 18% for the dataset Ber1b where the image noise was reduced by applying the EPS filter. The majority of the pores (>98%) was found to be connected on the basis of the open-closed porosity approach. The watershed algorithm applied to cases Ber1a-c did not have any influence on the porosity or the permeability tensor. Instead the number and trend of the modeled grain boundaries by using the binseparate function revealed a strong impact on the effective P-wave velocities that varied from 3706 to 5043 m/s. All results are shown in Figure 6, where a representative 2D slice of each case is shown, revealing the effect of filtering and assignment of grain boundaries. Comparing the P-wave velocitiy, porosity, and permeability sustained by digital rock analysis with results from lab investigations performed on this Berea sample (Madonna et al., 2012), we found the best matching dataset to be Ber1b filtered with EPS. Digital rock analysis yielded a total porosity of 18% and a permeability of 150 mD for Ber1b. The worst matching dataset for determination of effective physical properties were the unfiltered and the 3DM filtered one with a total porosity of 12% and permeabilities lower than 100 mD.

Conclusions

SRXTM is a non-destructive imaging method providing ultrahigh-resolution 3D volumes of rocks. The images from the TOMCAT synchrotron beam-line at the Swiss Light Source are characterized by resolutions down to 0.38 μm, allowing for a detailed study of the rock microstructure. SRXTM adds another level of detail compared to conventional micro-CT. Unfortunately, synchrotron facilities are not easily available to a broad scientific community. Therefore, we provide SRXTM raw data of various rock types described in Cases 1-9 (http://www.rockphysics.ethz.ch/downloads), together with descriptions of imaging conditions and laboratory characterization of the rock samples (Madonna et al., 2013). The provided data should stimulate many types of further investigations, for example, on image analysis methods, segmentation algorithms, numerical fluid flow calculations, or studies on mechanical rock properties.

In addition, we presented and discussed image filtering and a segmentation technique, followed by numerical computations of permeability and velocities. Even for SRXTM images, the resolution might be too low or the image noise is hampering the detection of grain-to-grain

contacts, as the image is used as a direct input for the determination of effective physical properties. We demonstrated that image noise filtering has a crucial influence on porosity and permeability, as well as on the modeled effective elastic properties and must be used with caution. For further investigations we suggest to (1) choose tools appropriate for the initial 3D image, (2) use workflows that are reproducible, (3) try different techniques and default values to find the best match. Further investigations need to be conducted for a good overview on all effects and for other rock types.

References

Dvorkin, J., Derzhi, N., Diaz, E. and Fang, Q. [2011] Relevance of computational rock physics: Geophysics, 76, E141–E153, doi: 10.1190/geo2010-0352.1.

Iassonov, P., Gebrenegus, T. and Tuller, M. [2009]: Segmentation of X-ray computed tomography images of porous materials: Water Resour. Res., 45, W09415.

Madonna, C., Almqvist, B. S. G., and Saenger, E. H. [2012] Digital rock physics: Numerical prediction of pressure-dependent ultrasonic velocities using micro-CT imaging: Geophysical Journal International, 189, 1475-1482, doi: 10.1111/j.1365-246X.2012.05437.x.

Madonna, C., Quintal, B., Frehner, M., Almqvist, B. S. G., Tisato, N., Pistone, M., Marone, F. and Saenger, E. H. [2013] Synchrotron-based X-ray tomographic microscopy for rock physics investigations: Gephysics, 78, D53-D64, doi: 10.1190/GEO2012-0113.1.

Saenger, E. H. [2008]: Numerical methods to determine effective elastic properties: International Journal of Engineering Science, 46, 598–605.

Shulakova, V., Pervukhina, M., Müller, T. M., Lebedev, M., Mayo, S., et al. [2013]: Computational elastic up-scaling of sandstone on the basis of X-ray micro-tomographic images: Geophysical Prospecting, 1-15.

Table 1. Experimental conditions and characteristics of the raw data

Case	Beam energy	Exposure time	Size of datacube	Magnification	Voxel size	Pixel depth
1	26 keV	500 ms	1024×1024×1024	10×	$(0.74 \ \mu m)^3$	16 bit
2	26 keV	300 ms	1024×1024×1024	20×	$(0.38 \ \mu m)^3$	16 bit
3	26 keV	500 ms	1024×1024×1024	10×	$(0.74 \ \mu m)^3$	16 bit
4	26 keV	300 ms	1024×1024×1024	20×	$(0.38 \ \mu m)^3$	16 bit
5	26 keV	500 ms	1024×1024×1024	10×	$(0.74 \ \mu m)^3$	16 bit
6	22.6 keV	300 ms	2048×2048×2048	20×	$(0.38 \ \mu m)^3$	8 and 16 bit
7	22.6 keV	300 ms	2048×2048×2048	20×	$(0.38 \ \mu m)^3$	8 and 16 bit
8	20 keV	100 ms	2048×2048×2048	10×	$(0.74 \ \mu m)^3$	16 bit
9	Polychromatic	1.4 ms	1008×1008×2016	~3.7x	$(2.96 \ \mu m)^3$	8 bit

Table 2. Numerical input parameters: P-Wave Modulus (M), Bulk Modulus (K), Shear Modulus (G) and Density (ρ)

Segmented class	M (GPa)	K (GPa)	G (GPa)	ρ (kg/m^3)
Quartz	96.98	37.8	44.3	2648
Calcite	115.97	73.3	32.0	2712
Grain boundary	9.70	3.8	4.4	2648
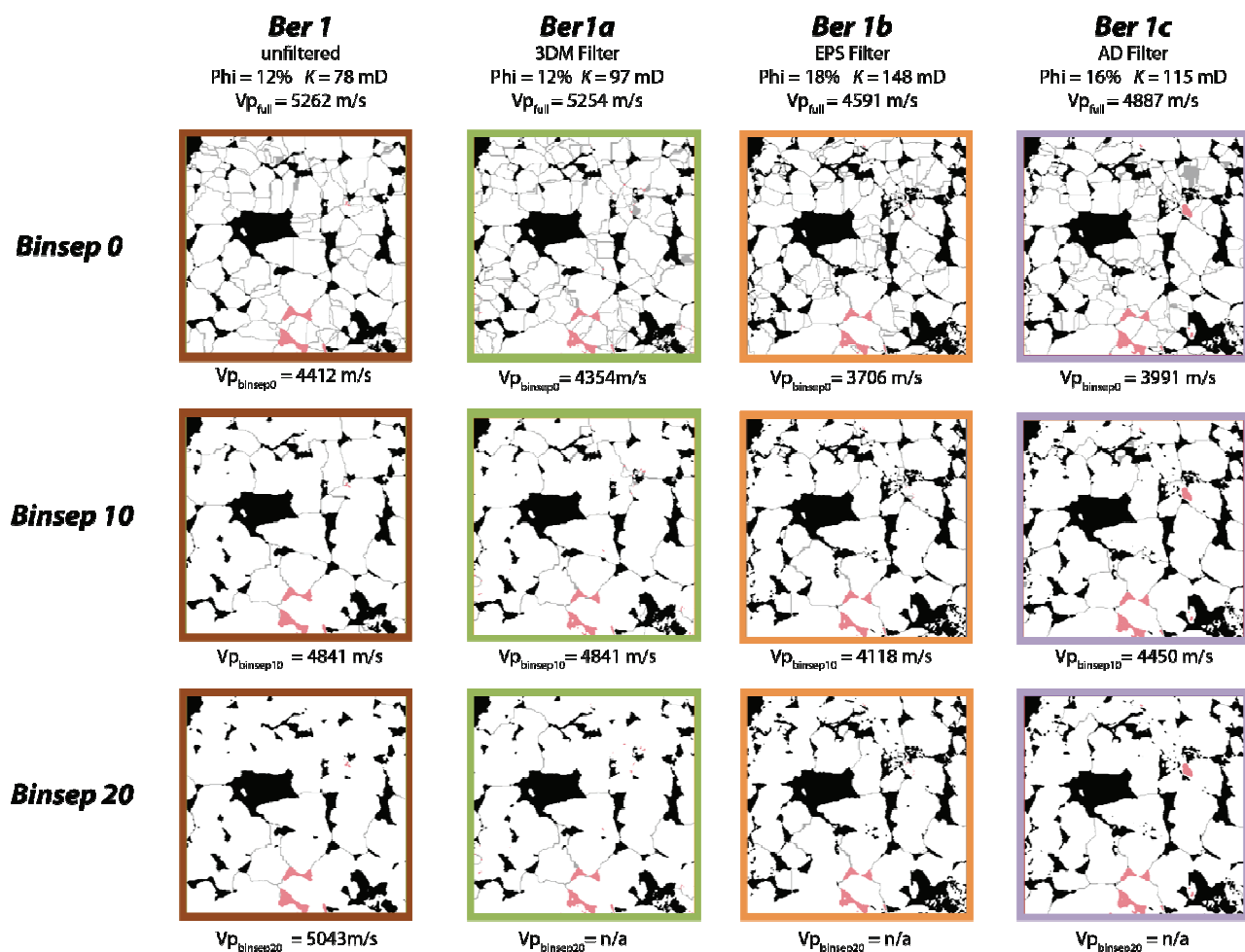
Figure 6. A representative 2D slice of each case depicting the different classes: pores – black, quartz – white, carbonate – pink and the grain-to-grain contacts – gray. For the different cases we estimated the porosity (Phi), the permeability (K), and two different P-wave velocities (Vp). For Vp_{full} we assigned the mineral moduli of Quartz to the grain boundaries. For Vp_{binsep} we used reduced moduli for the grain boundaries as given in Table 2.